Journal of Power Sources 209 (2012) 90–104

Contents lists available at SciVerse ScienceDirect

Journal of Power Sources

journal homepage: www.elsevier.com/locate/jpowsour

Mechanism of water transport in serpentine cathode channels of proton exchange membrane fuel cells

Yonghua Cai[a,*], Tao Chen[b], Tianqi Yang[a], Jinsheng Xiao[a]

[a] School of Automotive Engineering, Wuhan University of Technology, Hubei 430070, China
[b] School of Mechanical and Electronic Engineering, Wuhan University of Technology, Hubei 430070, China

ARTICLE INFO

Article history:
Received 19 December 2011
Received in revised form 22 February 2012
Accepted 23 February 2012
Available online 3 March 2012

Keywords:
Water motion
Hydrophilicity
Hydrophobicity
Surface tension
Channel
Fuel cell

ABSTRACT

The water motion in a simplified serpentine channel is investigated to study the dynamic water behavior in the serpentine channel in a proton exchange membrane fuel cell (PEMFC). The effects of corner shapes, the number of water inlet pores, the air inlet velocity and the water inlet velocity on the removal of water are discussed. Results show that the water drains out more quickly in a channel with a round corner than in a channel with a sharp corner. A channel with hydrophobic walls has both a higher water removal frequency and higher water coverage on the bottom wall than does a channel with hydrophilic walls.

1. Introduction

Water management is of great importance for a PEMFC operating at the normal temperature (80 °C). Low water content in the membrane causes low proton conductivity and consequent the bad performance of a PEMFC, while too much water leads to "flooding" that will block the diffusion of the reactant gas and eventually worsens the performance of a PEMFC. Now more and more research works focus on the dynamic behavior of water in a PEMFC, especially water motions in channels.

There is an abundant body of literatures on water management of PEMFCs in both experiments [1] and numerical simulations. Researchers utilize numbers of techniques to investigate the water transport inside fuel cells, including direct optic observation [2–9], neutron imaging [10–13], X-ray radiography [14,15], MRI [16], THz imaging [17], O_2-sensitive dye films [18] and water sensitive paper [19]. These researches mainly focus on the process in which water generates from the gas diffusion lay (GDL) to channels and in which water moves inside cathode channels and provide a good understanding for the water behavior inside fuel cells.

Numbers of modeling works mainly focus on the water management of fuel cells [20–27] and the GDL [28–35]. Some other modeling works investigated the motion of given water droplets/films in channels. Quan et al. studied different given water droplet/film distributions under different fuel cell operating conditions to obtain the water behavior inside a serpentine micro-channel [36]. Five cases with different initial water distributions in a serpentine channel are studied. Zhan et al. studied the effect of hydrophilicity of a graphite plate and the hydrophobicity of a GDL on the motion of a given water droplet/film in a straight channel and a serpentine channel [37]. Results show that the hydrophilicity of channel and the hydrophobicity of the GDL play an important role in the liquid water motion. Jiao et al. investigated air–water flow behaviors inside serpentine flow channels [38]. Cases with five spherical water droplets and water films with a thickness of 0.2 mm attached to different places in channels are studied. Result shows that water distribution and pressure drop vary in these five cases. Akhtar and Kerkhof studied the dynamic behavior of liquid water transport in the cathode with a tapered channel design [39]. The motion of a liquid water droplet of spherical shape with a volume of 0.268 mm^3 suspended in the center of the channel is investigated. Results show that hydrophobic top and side channel walls and a hydrophilic bottom wall are helpful to remove water. Kim et al. studied the effects of geometries and surface properties of flow channels on the liquid water exhaust capabilities [40]. Motions of two water droplets with a total volume of 1.0 μl assumed to initially exist inside the flow channels are studied. Results show that hydrophobic channels exhausted liquid water much faster than did hydrophilic channels, but the stagnant

* Corresponding author. Tel.: +86 13476146123; fax: +86 02787859247.
E-mail addresses: yhcai@whut.edu.cn, caitrans@163.com, caiyonghua@gmail.com (Y. Cai).

0378-7753/$ – see front matter © 2012 Elsevier B.V. All rights reserved.
doi:10.1016/j.jpowsour.2012.02.095

liquid volume in corners of hydrophobic channels was larger than that of hydrophilic channels. Le and Zhou investigate the behavior of water droplets in serpentine channels [41]. Motions of eight water droplets initially attached in the inlet part of channels are studied. Results show that the flow is unevenly distributed and that small droplets remain in the corners of the channel. Le et al. also indicate that the eight water droplets affect the motion of each other. Above works made an insight in the water motion in channels of a PEMFC. However, these works focus only on the behavior of pre-existed water droplets/films in channels, without considering the consecutive emergence of water from the GDL to channels.

Recently, studies on the motion of water generating from the GDL are carried out. Quan and Lai studied effects of the hydrophilicity of channel surfaces, the channel geometry and the air inlet velocity on water behaviors in a channel in which water generates from the whole surface of the GDL [42]. Results show that compared with a round corner channel, a sharp corner channel could be a better design. Ding et al. investigated gas–liquid two-phase flow patterns in cathode channels [43]. The water motion in a channel with 320 pores on the GDL surface with the same diameter of 400 μm is simulated. Results show that using a more hydrophobic GDL surface is helpful to expel water from the GDL surface, but may also increase the pressure drop. Zhu et al. studied the dynamic behavior of liquid water entering a straight channel through a GDL pore via a 2D model. Effects of channel size and pore size are taken into account [44,45]. On second thoughts, Zhu et al. studied the dynamic behavior of liquid water entering a straight channel through a GDL pore via a 3D model. Effects of static contact angle, air flow velocity, water injection velocity and dimensions of the pore are studied [46]. Results show that hydrophobic walls result in earlier detachment of water droplets, while hydrophilic walls results in spreading of the water droplet on the GDL surface. Le et al. studied liquid water behaviors in a proton exchange membrane fuel cell cathode with serpentine channels [47]. Results show that key factors that determined the shapes and behaviors of the droplets are the velocity of the air flow, the contact angle, the surface tension, and the viscosity of the droplet. Ding et al. also studied water motions in five different water injection structures [48]. Results show that more hydrophobic GDL surface and/or more hydrophilic channel walls would be helpful to remove the liquid droplets from the GDL surface to the channel walls. These works focus on the behavior of the water emerging from the GDL and provide a good understanding of the dynamic water behavior. However, these works focus on the water behavior in a straight cathode channel with only one water injection pore or water behavior in a channel with a whole surface generating water.

In the present work, we aim to investigate the effect of water emerging from one pore on the formation of and subsequent the behavior of water emerging from other pores and the effects of the hydrophobicity/hydrophilicity of channel walls, the shape of the corner, the air inlet velocity and the water inlet velocity on the water behavior and to investigated the volume fraction of water inside the channel chamber and the facet fraction of water on the bottom wall to study the mechanism of the water transport in serpentine cathode channels.

2. Numerical models

2.1. VOF model

The VOF model is used to model liquid and gas fluids by solving a single set of momentum equations and tracking the volume fraction of each of the fluids throughout the domain.

The tracking of the interface(s) between the phases is accomplished by the solution of a continuity equation for the volume fraction of one (or more) of the phases. For the qth phase, this equation has the following form [49]:

$$\frac{1}{\rho_q}\left[\frac{\partial}{\partial t}(\alpha_q\rho_q)+\nabla\cdot(\alpha_q\rho_q\vec{v}_q)=S_{\alpha_q}+\sum_{p=1}^{n}(\dot{m}_{pq}-\dot{m}_{qp})\right] \quad (1)$$

where α, ρ, v, $S_{\alpha q}$, $\dot{m}_{pq}$ and $\dot{m}_{qp}$ are volume fraction, density, velocity, source term, mass transfer from phase q to phase p and mass transfer from phase p to phase q, respectively.

The momentum equation is shown below:

$$\frac{\partial(\rho\vec{v})}{\partial t}+\nabla\cdot(\rho\vec{v}\vec{v})=-\nabla p+\nabla\cdot[\mu(\nabla\vec{v}+\nabla\vec{v}^T)]+\rho\vec{g}+\vec{F} \quad (2)$$

where μ, p, F and T are stand for dynamic viscosity, pressure, source term and temperature.

The energy equation, also shared among the phases, is shown below:

$$\frac{\partial}{\partial t}(\rho E)+\nabla\cdot(\vec{v}(\rho E+p))=\nabla\cdot(k_{\text{eff}}\nabla T)+S_h \quad (3)$$

where k_{eff}, S_h and $E=\sum_{q=1}^{n}\alpha_q\rho_q E_q/\sum_{q=1}^{n}\alpha_q\rho_q$ are effective thermal conductivity, source term and energy.

Surface tension is a force, acting only at the surface, that is required to maintain equilibrium in such instances and is shown below:

$$p_2-p_1=\sigma\left(\frac{1}{R_1}+\frac{1}{R_2}\right) \quad (4)$$

where p_1 and p_2 are the pressures in the two fluids on either side of the interface, σ is the surface tension coefficient, R_1 and R_2 are the radii in orthogonal directions.

The force at the surface can be expressed as a volume force and it is the source term, which is added to the momentum equation. It has the following form:

$$F_{\text{Vol}}=\sigma_{ij}\frac{\rho k_i\nabla\alpha_i}{0.5(\rho_i+\rho_j)} \quad (5)$$

where $k=\nabla\cdot(n/|n|)$ is surface curvature.

2.2. Geometric model

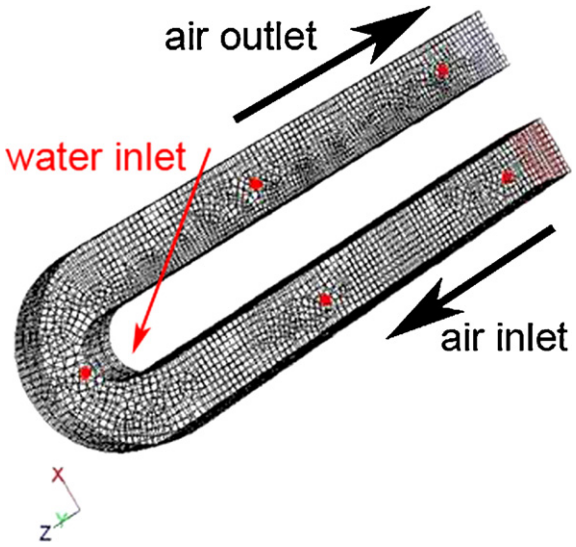

Fig. 1. Schematic of the computational domain.

Fig. 1 shows a schematic illustration of the computational domain and corresponding mesh. In the baseline case, a round corner channel with 1 mm × 1 mm square cross section and 4 mm

in length and the rib with 1 mm in width are applied. Five water inlet pores with 0.2 mm diameter are attached to the bottom wall of the channel (the interface between a channel and a GDL). The length of the channel and the size and the location of the pores are determined according to experimental observations [46,50–52]. A computational mesh consisting of 21,460 cells is used for the baseline case. The adequacy of this grid was tested by increasing and decreasing the number of grid nodes by ±20%, and similar transport processes were obtained.

2.3. Boundary and initial conditions

In the baseline case simulations, an air velocity of 10 m s^{-1} normal to the boundary at 0 bar (gauge pressure) and a water velocity

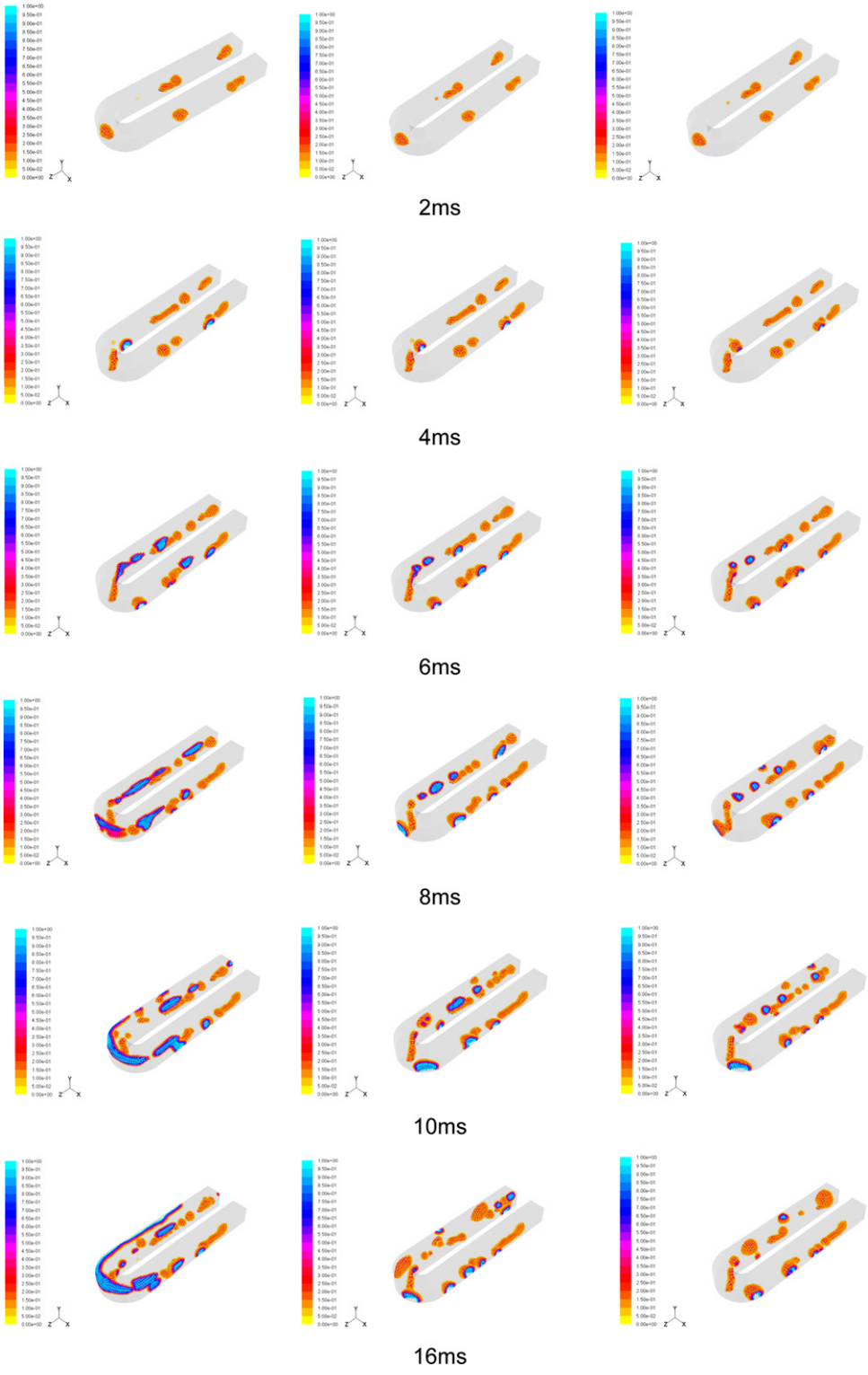

Fig. 2. Water motion in the channel in the baseline case.

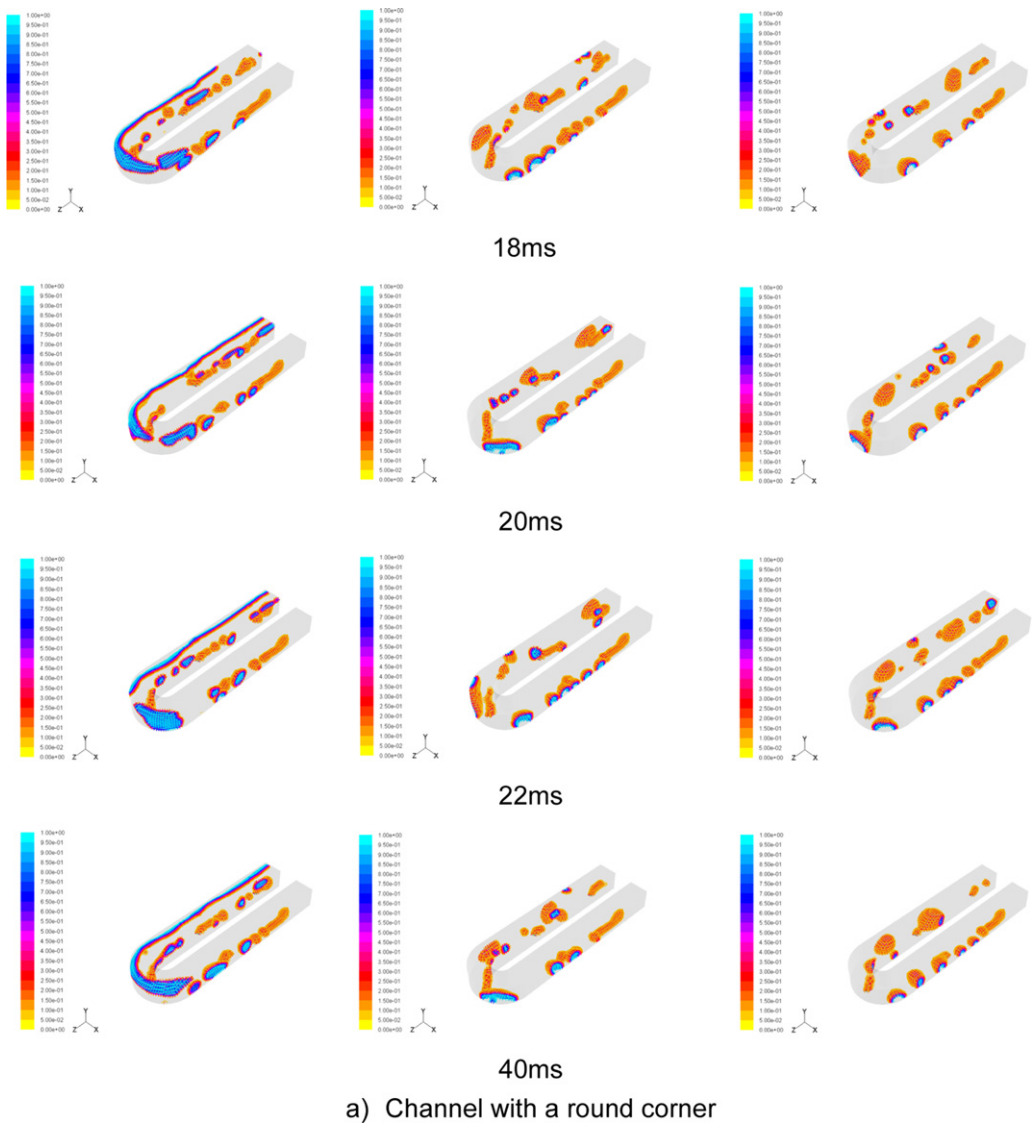

Fig. 2. (*Continued*).

of 1 m s^{-1} normal to the boundary are applied. The operating temperature is set to 300 K. The static contact angle of the bottom wall of the channel is set to 135°, standing for the typical PTFE treatment of a GDL. Velocities of air and water are also set corresponding to the normal vehicular PEMFC stacks condition to simulate real operating environments [45,46].

3. Results and discussion

Water dynamic behaviors in a cathode serpentine channel with five water inlet pores are simulated. Effects of hydrophilicity/hydrophobicity of channel walls, corner shapes and velocities of air and water on the water transport are discussed. The values of the static contact angles of the channel walls are set to 45°, 90° and 135°, respectively, in the cases.

3.1. Baseline case

3.1.1. Water motion in the channel with a round corner

3.1.1.1. Static contact angle 45°. Fig. 2 shows water dynamic behaviors in the channel with hydrophilicity/hydrophobicity walls at different times (From left to right, the static contact angles are set to 45°, 90° and 135°, respectively). It can be seen that water motions are similar at the first stage in all channels (0–6 ms) but differ at 8 ms. At the beginning, water moves toward one side of the channel due to the blockage effect of the corner. Like that in a straight channel [46], the water is tore into droplets before it moves to the next water injection pore because of the hydrophobicity of the bottom wall and the shearing force of the inlet air. When these newly formed water droplets move to the next water injection pore, they collide with the water droplet emerging and are pushed to the outside wall of the channel by the shearing force of the air. Counteracted by the collision force and the air shearing force, the surface tension of the water cannot maintain the shape of the water as a droplet anymore. Water droplets are dragged into long, thin water films and ascend to the boundary of the side wall and the top wall of the channel. These long, thin water films merge into long, thick films and move along the boundary at 16 ms. Water emerging from pores at inlet part of the channel ascends to the boundary of outside wall and the top wall and eventually moves along the boundary because of the inertia force and the hydrophilicity of the outside and top wall. On the contrary, water emerging from the corner and the outlet part of channel ascends to the boundary of the inner side wall and the top wall of the channel. Water emerging from the inlet part of the channel begins to drain out of the channel at 18 ms. Water motions in the channel are almost the same after 16 ms.

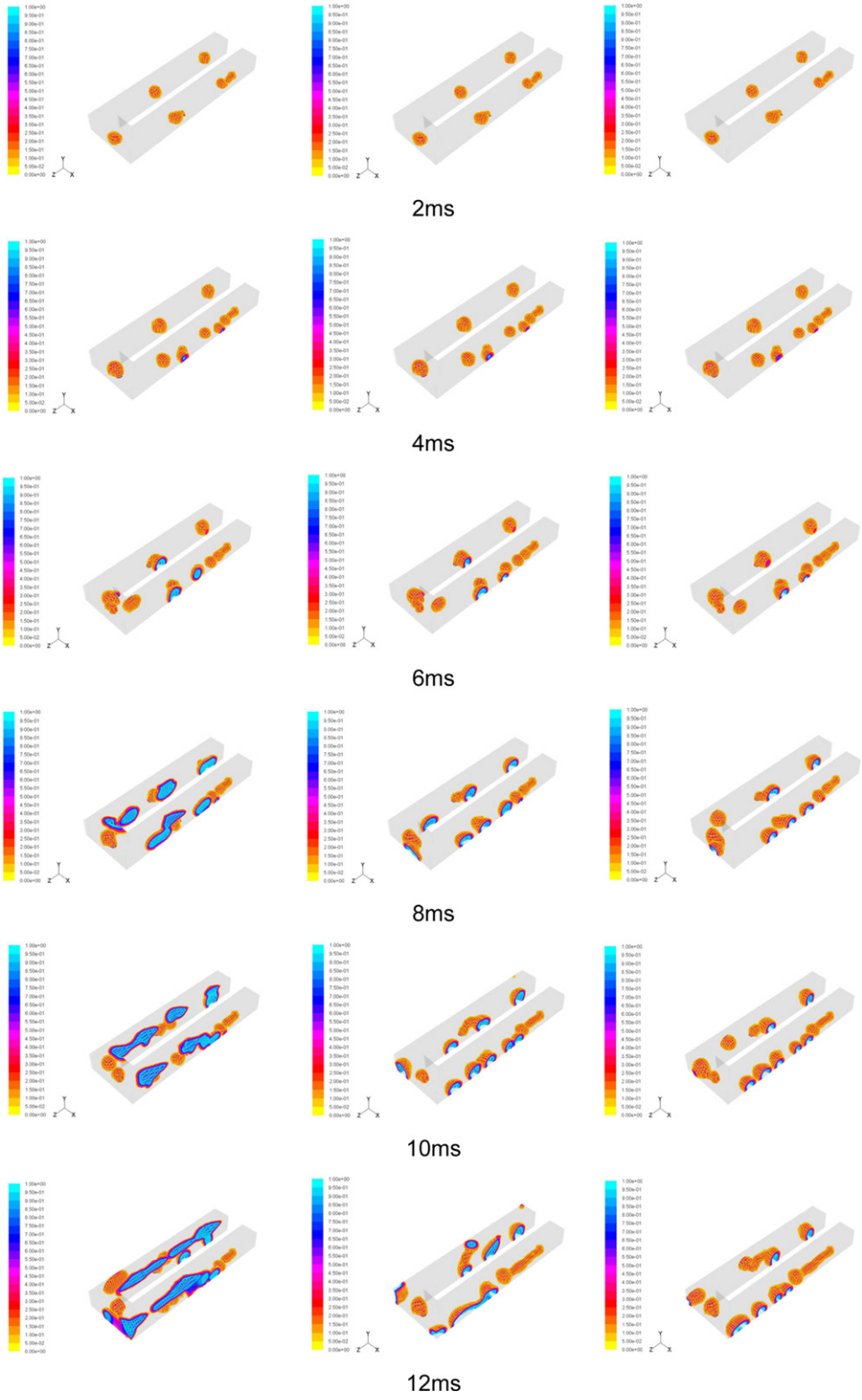

Fig. 2. (*Continued*).

3.1.1.2. Static contact angle 90° and 135°. Unlike those in the channel with hydrophilic walls, water shapes in the channel with walls with the static contact angel set to 90° are mainly in the form of droplets. In the channel with hydrophilicity side and top walls, contact surface between water droplets and the side and top walls begins to expand after 6 ms because of the hydrophilicity of the walls. However, in the channel with walls with the static contact angel set to 90°, the surface tension of water maintains the shape of droplets because the hydrophilicity force of the walls is less than the surface tension of water. When the water droplet moves to the next water inject pore, it collides with the water emerging from the pore and become a bigger one. Bigger water droplets begin to form after 16 ms. Adhering to the outside wall by the inertial force and the air shearing force, water droplets emerging from the inlet part

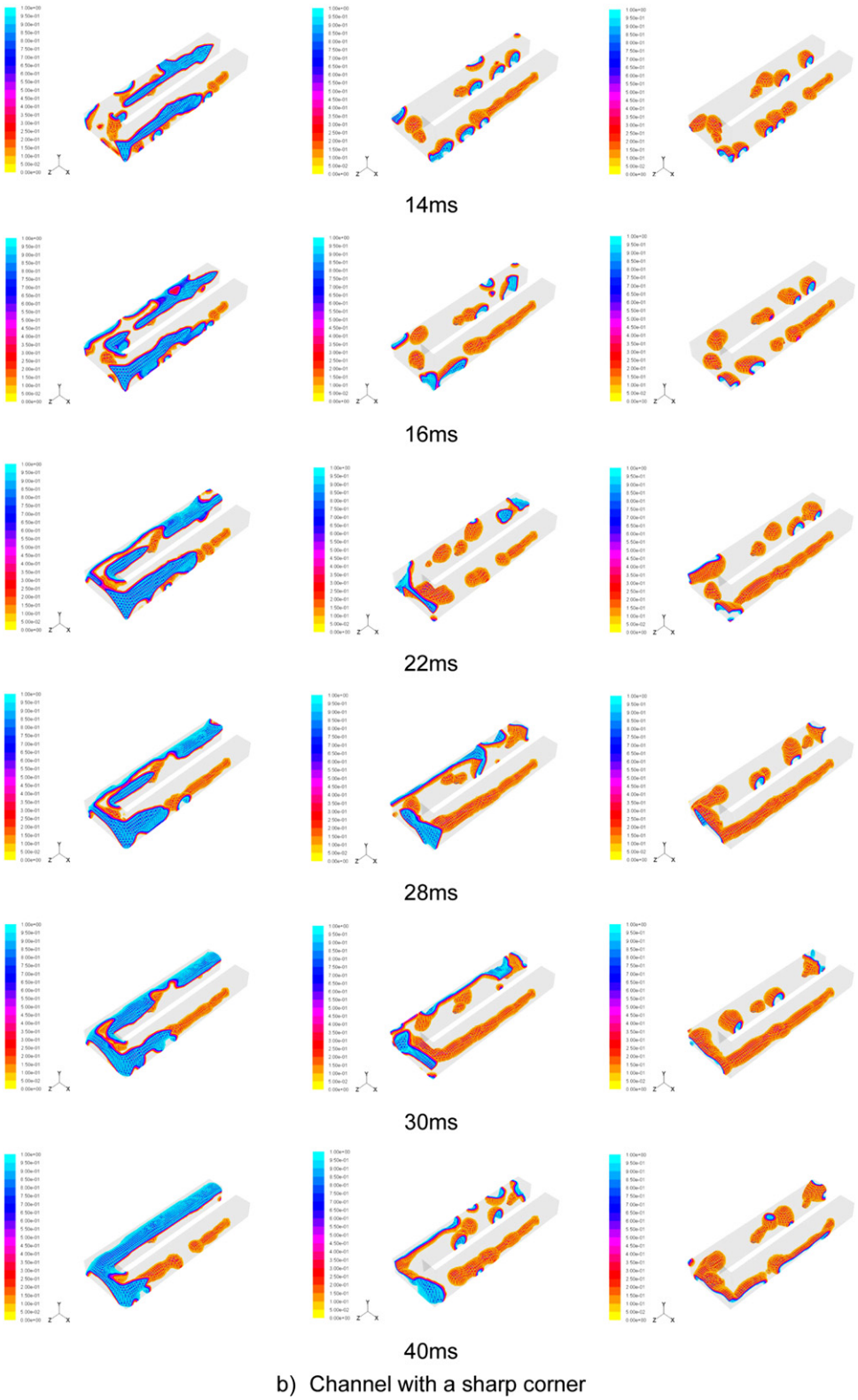

Fig. 2. (*Continued*).

of the channel drain out of the channel. Although water droplets emerging in the corner and the outlet part of channel adhere to the inside wall of channel, dynamic behaviors of water droplets emerging both in the corner and outlet part and in the inlet part of the channel are almost the same. Water motion in the channel with walls with the static contact angel set to 135° is similar to that in the channel with walls with the static contact angel set to 90°.

3.1.2. Water motion in the channel with a sharp corner

3.1.2.1. Static contact angle 45°. Duo to the blockage of the sharp corner, the pressure in the corner part of the channel with a sharp

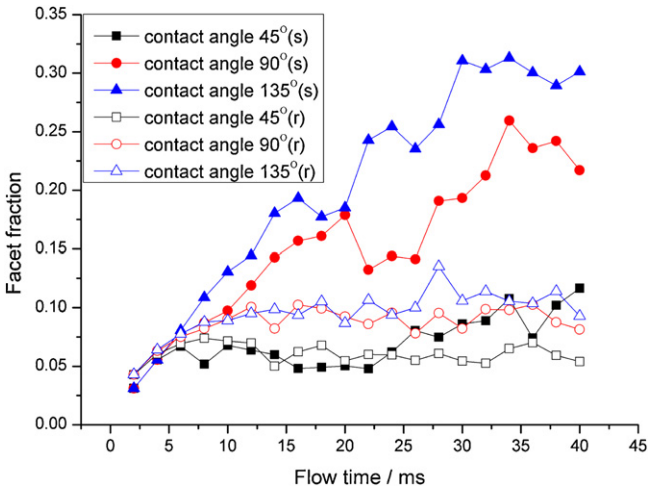

Fig. 3. Facet fraction of water on the bottom wall of the channel.

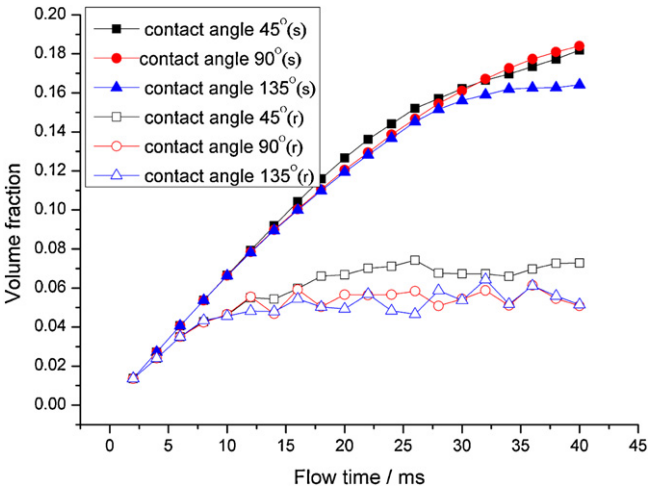

Fig. 4. Volume fraction of water inside the channel.

corner is greater than that in the channel with a round corner. At the very beginning, the water behavior in the channel with a sharp corner is similar to that in the channel with a round corner, as shown in Fig. 3. Water emerging in the inlet part of the channel moves to the outside wall of the channel and finally forms a long, thin water film under the effect of the hydrophilicity of the outside wall and the shearing force of the inlet air at 8 ms. With the further water generation, water films moving along outside wall ascend to the boundary of the outside wall and the top wall under the shearing force of the inlet air. When the water films move to the corner, water emerging at the corner part merges with these water films, so does the water emerging in the outlet part of the channel. Since the water film is long and relatively thin, the hydrophilicity of the top wall and the air shearing force are greater than the gravity of the water film. So the long, thin water films can move on the top wall of the channel. Finally, water films move along and cover the whole top wall from the corner part to the outlet part of the channel at 14 ms.

3.1.2.2. Static contact angle 90°. With the decrease of hydrophilicity of walls, water emerging from the pores forms water droplets rather than water films. When water droplets moves to the sharp corner, the blockage of the sharp corner and these water droplets themselves forms a high pressure area in the corner part. Water droplets in the inlet part of the channel move slowly and finally merge into one long, thick water film at 12 ms. When the water film moves through the corner into the outlet part of the channel, it collides with water emerging in the corner and the outlet part of the channel and forms a thicker film. Most space inside the channel is occupied by this long, thick water film. Water behavior in the outlet part of the channel is quite different from that in the inlet part. Water exists almost in the form of droplets during the whole drainage process.

3.1.2.3. Static contact angle 135°. The water motion in the channel with walls with the static contact angel set to 135° is similar to that in the channel with walls with the static contact angel set to 90°, but water droplets are bigger and water films are thicker. Long thick water films occupy almost the whole inlet part and the corner part of the channel while the outlet part of the channel is occupied by big water droplets. The blockage occurs more frequently because of thick water films in the inlet part of the channel and big water droplets in the outlet part of the channel.

Fig. 3 shows the facet fraction of water on the bottom wall of channels with other walls set to different static contact angles and with different corner shapers ('s' stands for a sharp corner and 'r' stands for a round corner). It can be seen that in all cases, the facet fraction of water on the bottom wall is less in the channel with a round corner than in the channel with a sharp corner. So the reactant gas diffuses better in the round corner channel than in the sharp corner channel and water emerges more easily in the round corner channel than in the sharp corner channel. The volume fraction of water inside the channel with a sharp/round corner can be found in Fig. 4. The round corner channel also has less water volume fraction than does the sharp corner channel. Due to the blockage of the sharp corner, water in the inlet part and the corner part moves slowly. So the water droplets in the inlet part of the channel tend to join each other to form even bigger ones. Due to the weaker air shearing force, the consecutive water injection and the slow movement of water droplets, water droplets on the hydrophobic bottom wall in the inlet part of the channel can connect with each other and eventually form long thick water films, so do the water droplets in the sharp corner part. Unlike the sharp corner, the round corner provides a good passage for both the air and the water. Due the stronger air shearing force, the quick water droplets movement and the hydrophobicity of the bottom wall, water droplets on the hydrophobic bottom wall are tore into smaller ones and move quickly out of the channel. It is more obvious in the case with the air inlet velocity set to 15 m s^{-1}, as shown in Fig. 5 . It can be seen that lots of smaller water droplets are formed by the shearing force even in the hydrophilic channel. Rather than forming long, thick water films, water films in the hydrophilic channel that attach the wall by the surface tension are cut by the strong shearing force into short, thin films and some small water droplets since the surface tension can only maintain a thin water film under the increased air shearing force.

However, it is interesting to found that the volume fraction of water inside the channel decreases with the increase of the static contact angle in the cases studied but the facet fraction of water on the bottom wall of the channel increase with the increase of the static contact angle. This finding suggests that unlike water in the channel with hydrophobic walls, water in the channel with hydrophilic walls locates inside the chamber of the channel, on the top wall of the channel or on the side walls of the channel rather than on the bottom wall of the channel. Although the channel with hydrophobic walls has the lowest volume fraction of water, more water droplets/films move on the bottom wall than do water droplets/films in the channel with hydrophilic walls. With the increase of the air and water inlet velocity, the difference of volume fraction of water inside the channel of the case studied

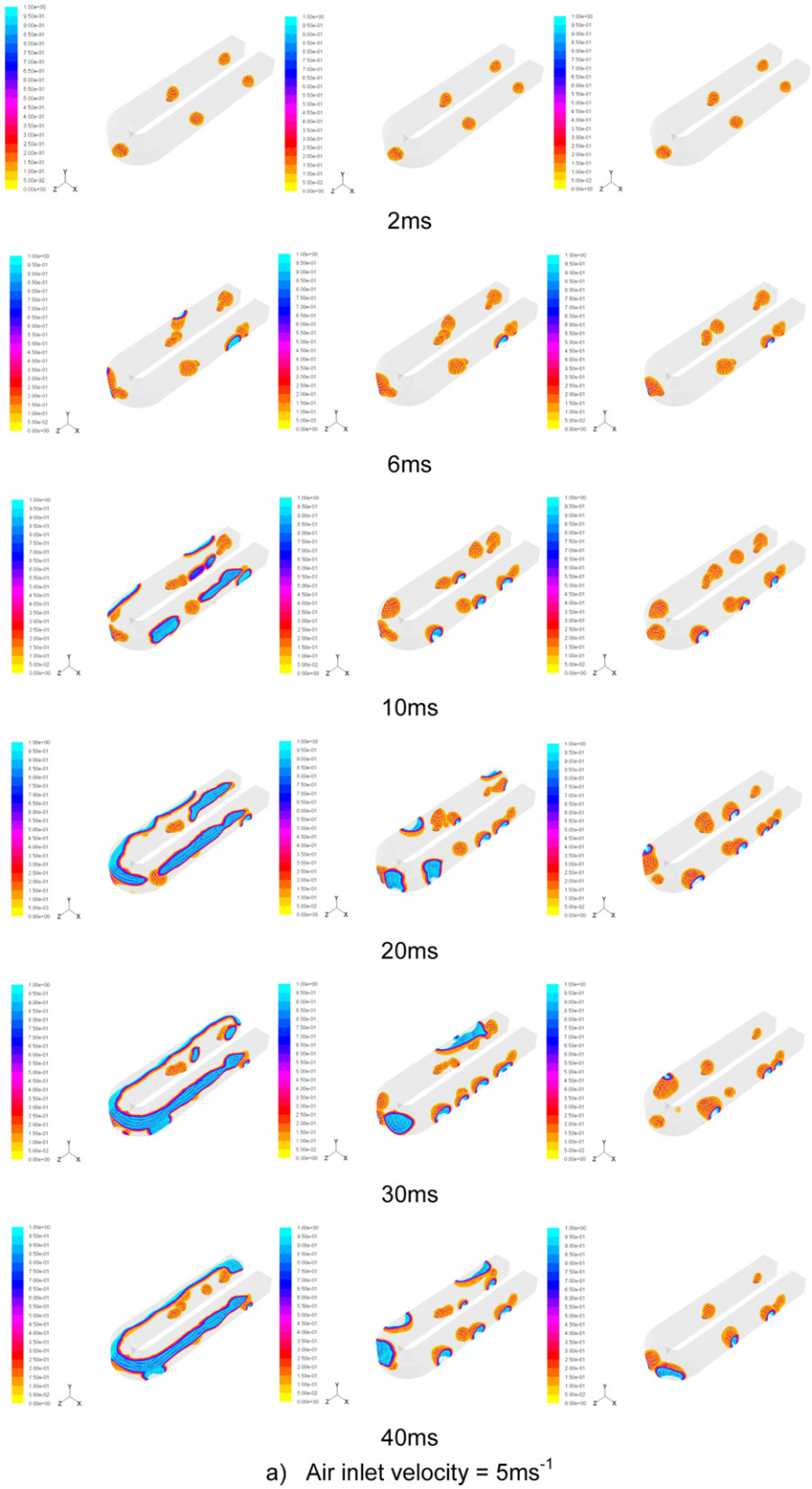

Fig. 5. Water motion in the channel under different air inlet velocities.

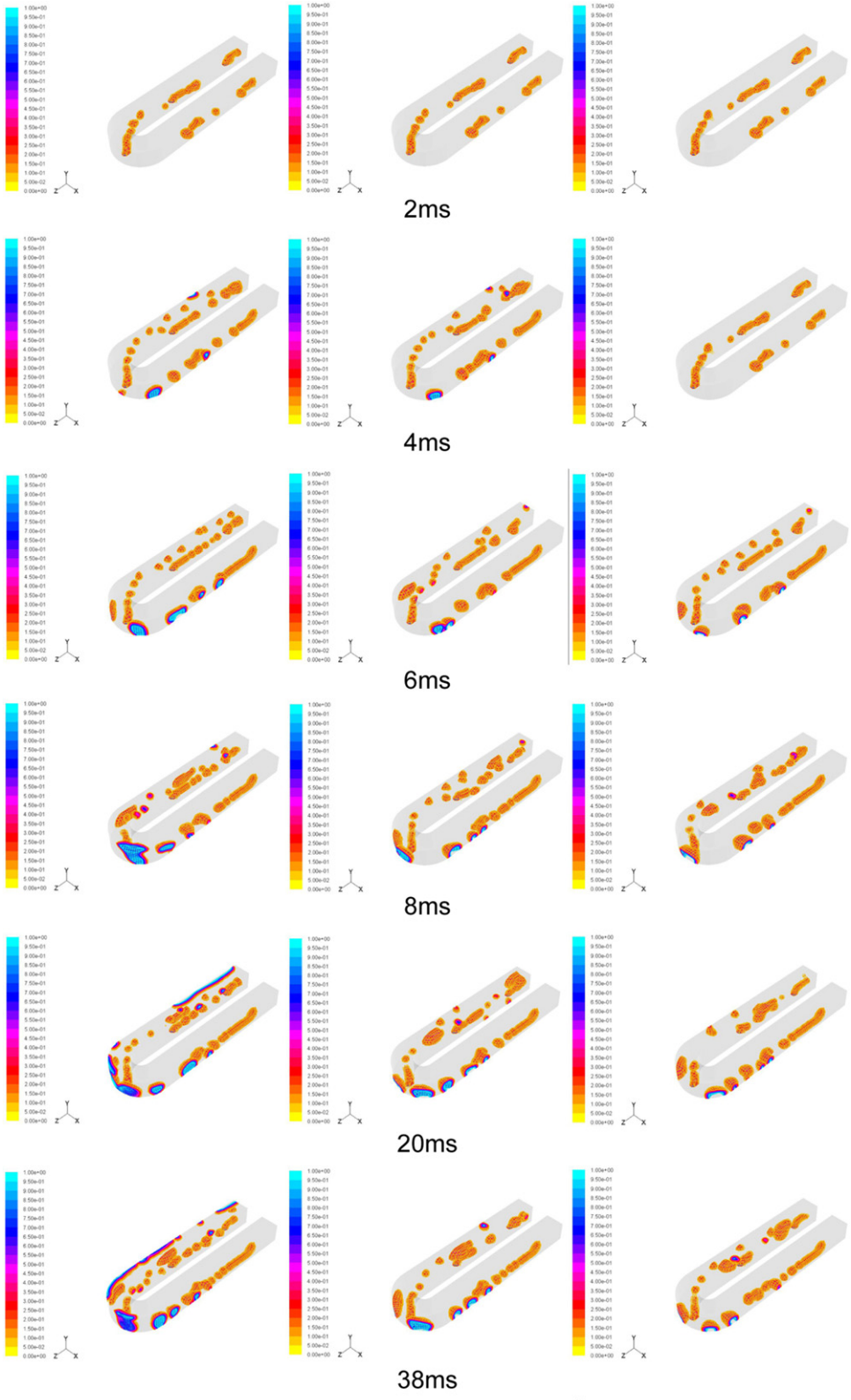

Fig. 5. (*Continued*).

decreases while the difference of facet fraction of water on the bottom wall maintains. So it may be helpful for fuel cells operating at high loads to expel water if the channel walls are hydrophilic since the more bottom wall areas are uncovered by water, the more reactant gas can pass from the GDL to the channel.

3.2. Effect of the air inlet velocity

Since the round corner channel performs better than the sharp corner channel, the discussion below is based on the round corner channel model.

3.2.1. Static contact angle 45°

The air inlet velocity has a significant effect on the dynamic behavior of water. Simulation cases in which the air inlet velocity set to 5, 10 and 15 m s^{-1} are studied to investigate water transport in the channel.

Results show that water motions at different air inlet velocities are quite different. Fig. 5 shows water motions at different air inlet velocities. When the inlet air velocity equals 5 m s^{-1}, water droplets emerging from inlet pores keep the shape of droplets because the shearing force of air is less than the surface tension of the water. Water droplets are elongated at a larger air inlet velocity. Water droplets attach to the sidewall of the channel at 4 ms because the hydrophilicity of the wall is greater than the shearing force of the air. Water emerging from the inlet part of the channel attaches to the outside wall at the very beginning and moves to the boundary part of the outside wall and the top wall. So does water emerging from the corner part. Finally, water emerging from the inlet part and the corner of the channel merges into one long, thin water film and moves along the boundary of the outside wall and the top wall. On the contrary, water emerging from the outlet part of the channel moves towards the boundary of the inside wall and the top wall and then drain out.

When the inlet air velocity reaches 15 m s^{-1}, the shearing force of the air is greater than that in the baseline case, so water emerging at the inlet part is tore into small water droplets. Small water droplets collide with each other and form several thin water films under the air shearing force and hydrophilicity of channel walls. Dragged by the inertial force, those water films form one long, thin film when they move through the corner. Water emerging in the corner is tore into many tiny water droplets and are blew out through the chamber without attaching to any wall of the channel. Unlike that of water emerging in the inlet part and the corner, motion of water emerging in the outlet part of the channel is mainly in the form of thick water films.

3.2.2. Static contact angle 90°

Compared to that in the baseline condition, the air shearing force is less when the inlet air velocity equals 5 m s^{-1}. Under a less shearing force, water emerging from the pores is inclined to form bigger water droplets under the surface tension. It can be seen that when water droplets move through the water inlet pores, they merge with the water emerging from the pore and form even bigger ones. Water motion in the channel is mainly in the form of big water droplets. Less hydrophilicity and greater shearing force lead to small water droplets in the channel when the air inlet velocity reaches 15 m s^{-1}. Even though water droplets collide with each other, newly formed water droplets are so small that they drain out of the channel quickly.

3.2.3. Static contact angle 135°

The water motion is similar to that in the channel with the static contact angle of walls set to 90° under both conditions. It can be seen that the difference of water motions in above cases diminishes with the increase of the air inlet velocity.

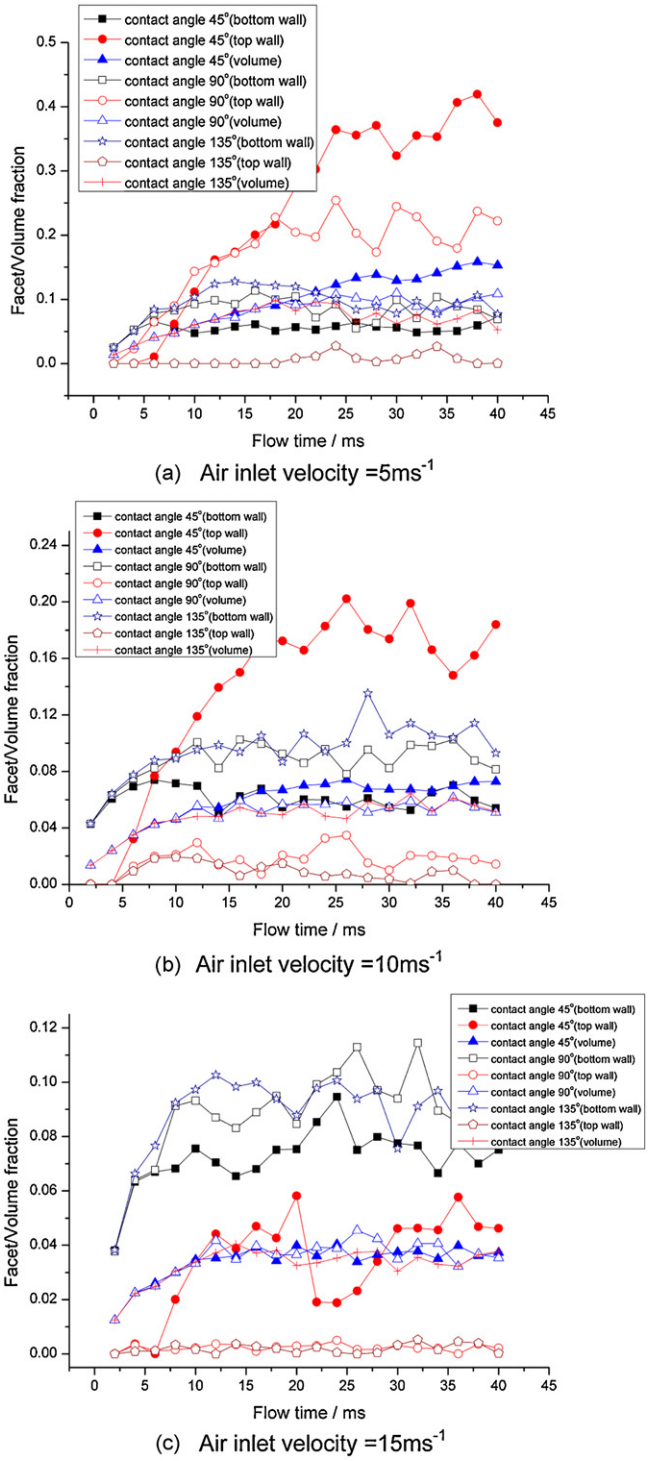

Fig. 6. Facet and volume fraction of water in the channel under different air inlet velocities.

Fig. 6 shows the volume fraction of water in the channel and the facet fraction of water on the walls of the channel under different air velocities. It can be seen that the volume fraction of water inside the channel drops with the increase of the static contact angle. The drop is noticeable when the air velocity increases from 5 m s^{-1} to 10 m s^{-1} but less significant when the air velocity increases from 10 m s^{-1} to 15 m s^{-1}. It also can be found that under different air velocities, the channel with wall static contact angle set to 45° has the least facet fraction of water on the bottom wall but the highest volume fraction of water inside the channel. Since the shearing

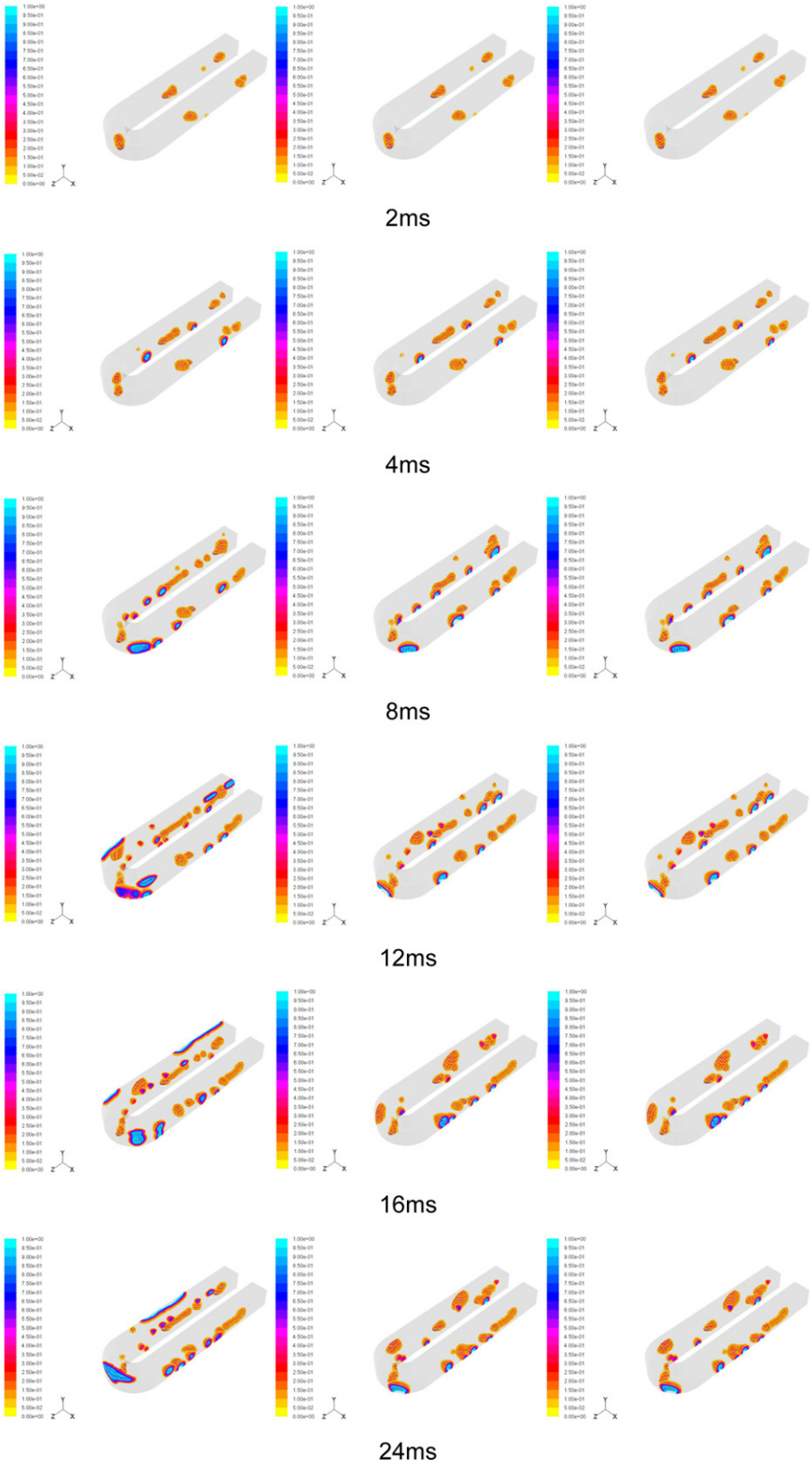

Fig. 7. Water motion in the channel under different water inlet velocities.

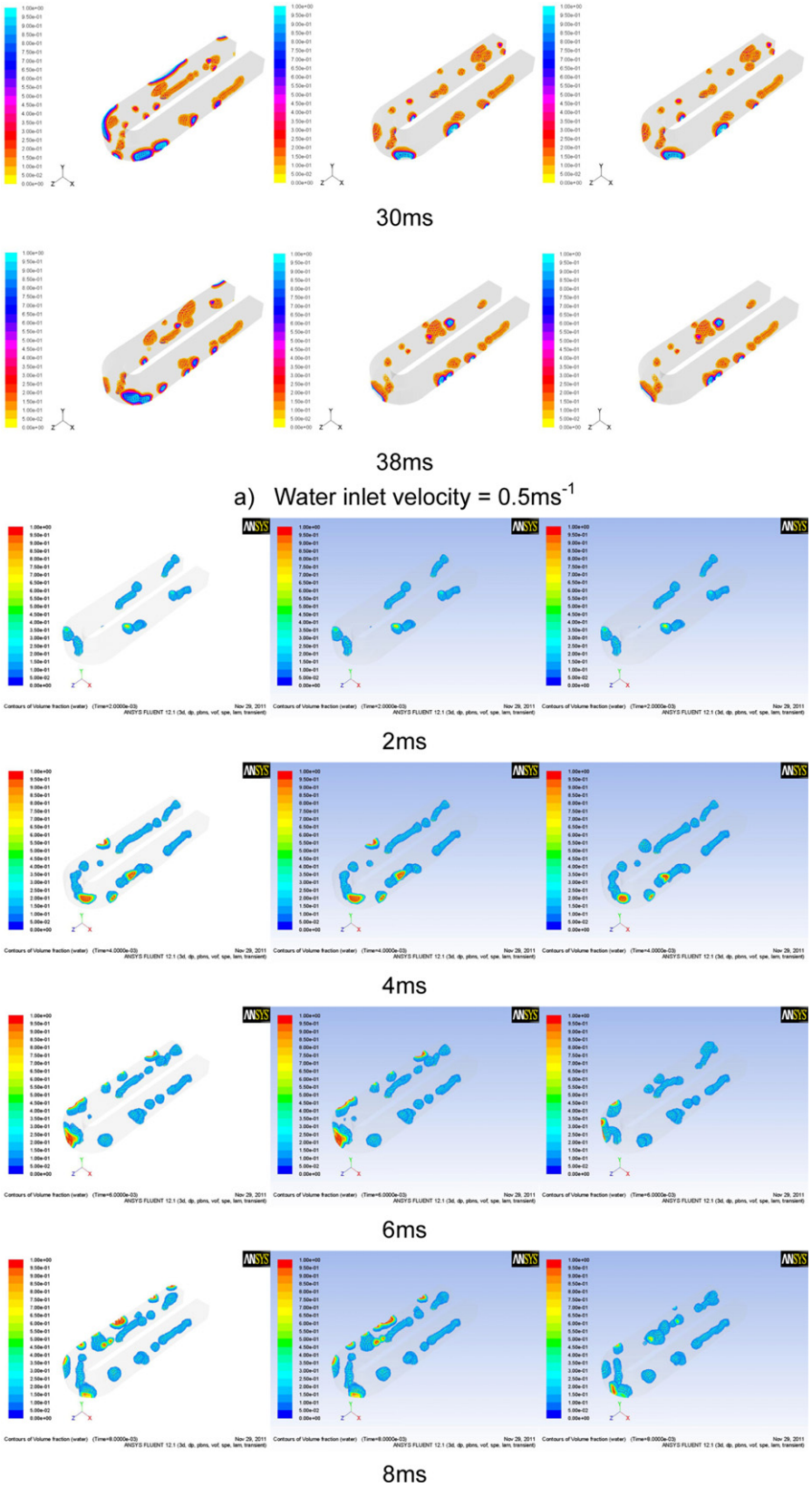

Fig. 7. (*Continued*).

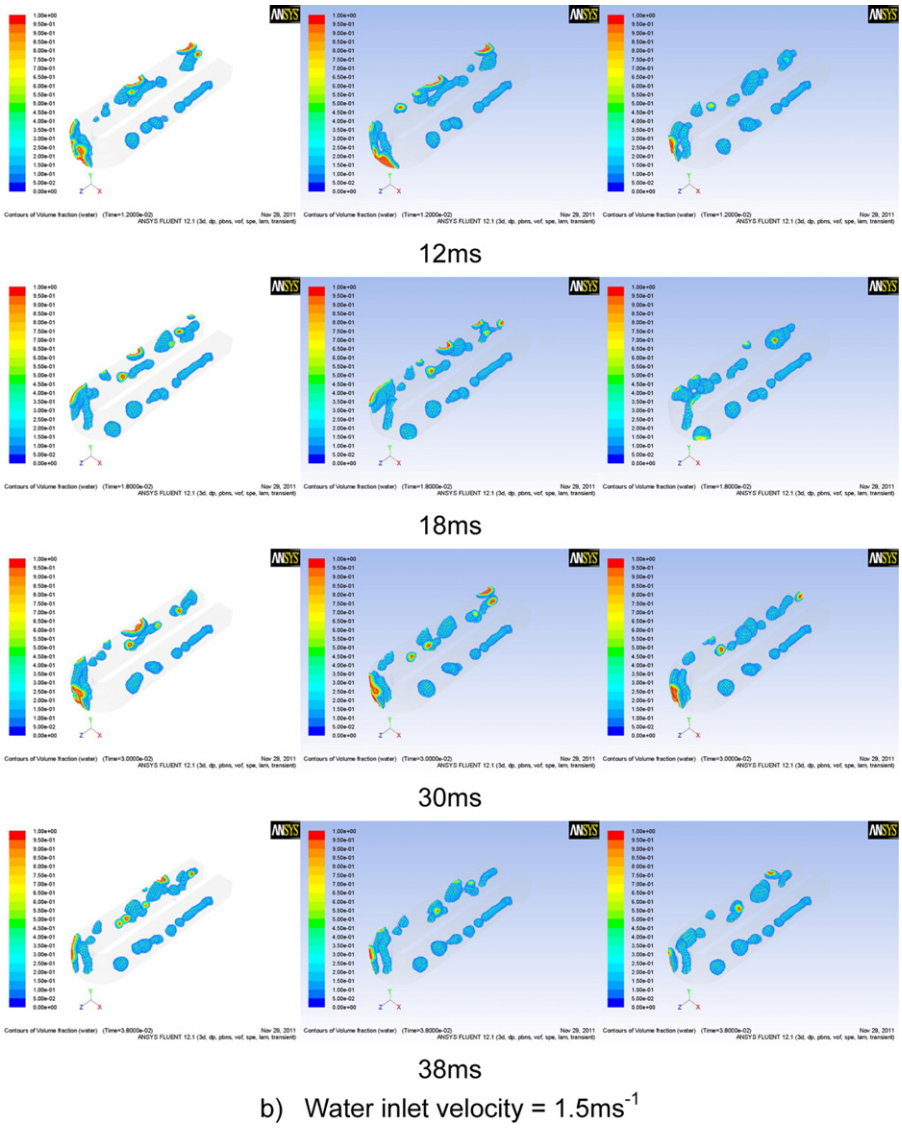

Fig. 7. (*Continued*).

force of the air is not great enough to counteract the effect of the surface tension of the water, water merges into thick films or big droplets under air velocity at 5 m s^{-1}. Water films and droplets are tore apart with the increase of the inlet air velocity. These thin, short films and small droplets are easier to drain out than are thick films and big droplets.

3.3. Effect of the water inlet velocity

3.3.1. Static contact angle 45°

Fig. 7 shows the water motion under different water inlet velocities. Under less water generating rate (0.5 m s^{-1}), water emerging from the pores is tore into many small water droplets. Unlike those in the baseline case, water droplets under this circumstance collide and form several water films rather than one long water film. Water emerging from the outlet of the channel exists mainly in the form of small water droplets. Water forms small water droplets at a high water generating rate (1.5 m s^{-1}). Water droplets collide and form many big water droplets rather than one water film.

3.3.2. Static contact angle 90°

The water motion in the channel with water generating rate at 0.5 m s^{-1} is also different from that in the baseline case. Water forms droplets more quickly than that in the baseline case. The size of the water droplets formed under collision in the inlet part of the channel is small. These water droplets move through the corner on the outside wall of the channel and finally drain out. When water generating rate equals 1.5 m s^{-1}, the water motion in the channel with the wall static contact angle set to 90° is almost the same as that in the channel with the wall static contact angle set to 45°.

3.3.3. Static contact angle 135°

Under this condition, water in the channel forms more water droplets at an earlier stage. Water drains out mainly in the form of small droplets. When water generating rate equals 1.5 m s^{-1}, the water motion in the channel with the wall static contact angle set to 135° is almost the same as that in the channel with the wall static contact angle set to 45° and 90° except for the size of the droplets. Because of the hydrophobicity of walls, water mainly moves on the bottom wall rather than on the side walls.

Fig. 8 shows the facet and volume fraction of water in the channel under different water inlet velocities. It is interesting to found that under all the conditions, the channel with water inlet velocity at 1 m s^{-1} has the highest water fraction on the bottom wall while the channel with the least water inlet velocity has the least water volume fraction. When the water inlet velocity is low, water

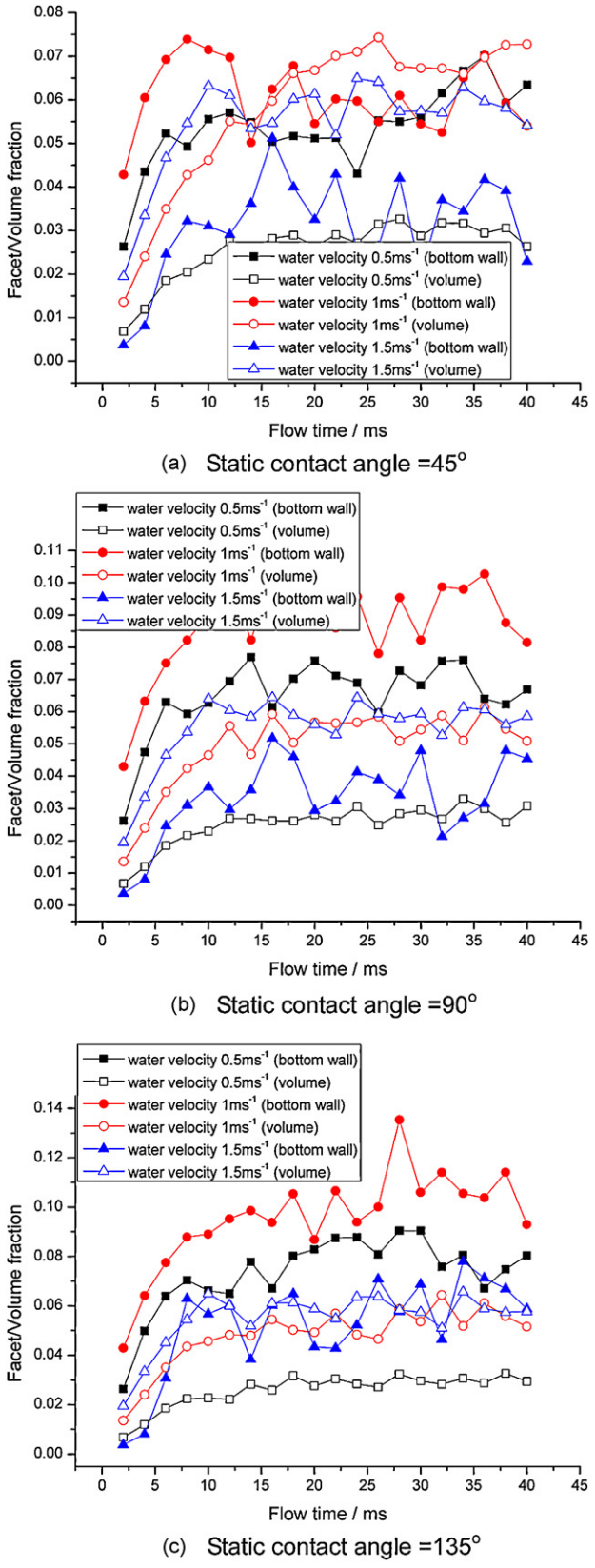

Fig. 8. Facet and volume fraction of water in the channel under different water inlet velocities.

entering the channel forms only small droplets or thin water films and the inertia force is not strong enough to push these droplets or films to the side wall or top wall. So the water droplets and films move through the channel mainly on the bottom wall. The volume fraction of water is less because water entering the channel in certain time is less due to the low water inlet velocity and because small droplets and thin films are easy to drain out of the channel. On the contrary, water forms larger droplets or thicker films when water inlet velocity increases. Under this circumstance, large water droplets or thick water films have more kinetic energy and are pushed toward the side wall or even the top wall. So water moves mainly on the side wall or on the top wall. Since, in a certain time, more water enters the channel under a high water inlet velocity and large droplets and thick films are hard to drain out of the channel, the volume fraction in the channel with a high water inlet velocity is greater than that in the channel with a low water inlet velocity.

Besides, the pressure loss in the channel is investigated and findings show that pressure loss increases with the increase of hydrophobicity of channel walls. In channel with hydrophobicity walls, water occurs mainly in the form of droplets as seen in Figs. 2, 5 and 7. Unlike the water films shaped in the channel with hydrophilic walls, water droplets in the channel with hydrophobic walls need more energy to move, resulting in more pressure loss. So water droplets in the channel with hydrophobic walls move out of the channel more quickly than the water films and water droplets in the channel with hydrophilic walls in the cost of more pressure loss. The results match those in both experimental and computational works [12,13,43].

4. Conclusions

The following conclusions can be obtained from above study.

1) Water drains out more quickly in a round corner channel than in a sharp corner channel. Water moves in the shape of thick films in the inlet and corner part of a sharp corner channel but in the shape of droplets in the inlet and corner part of a round corner channel.
2) The volume fraction of water inside the channel decreases with the increase of the static contact angle but the facet fraction of water on the bottom wall of the channel increase with the increase of the static contact angle. The formation and motion of water droplets/films in a channel with a corner are quite different from those in a straight channel.
3) Water emerging from one pore has a great impact on the formation of and subsequent on the behavior of water emerging from other pores. The formations and movements of water differ under different air inlet velocities, water inlet velocities and wall static contact angles, but the difference diminishes with the increase of the air inlet velocity.

Acknowledgements

The authors would like to acknowledge the support from National Natural Science Foundation of China (No. 50975214) and Hubei Provincial Natural Science Foundation of China (Grant No. 2011CDB431) for this study.

References

[1] A. Bazylak, Int. J. Hydrogen Energy 34 (2009) 3845–3857.
[2] X.H. Wang, T.V. Nguyen, J. Power Sources 197 (2012) 50–56.
[3] J.P. Owejana, T.A. Trabold, D.L. Jacobson, M. Arif, S.G. Kandlikar, J. Hydrogen Energy 32 (2007) 4489–4502.
[4] A. Turhan, S. Kim, M. Hatzell, M.M. Mench, Electrochim. Acta 55 (2010) 2734–2745.

[5] A. Turhan, K. Heller, J.S. Brenizer, M.M. Mench, J. Power Sources 160 (2006) 1195–1203.
[6] D. Spernjak, A.K. Prasad, S.G. Advani, J. Power Sources 170 (2007) 334–344.
[7] K. Nishida, T. Murakami, S. Tsushima, S. Hirai, J. Power Sources 195 (2010) 3365–3373.
[8] J.M. Sergi, S.G. Kandlikar, Int. J. Hydrogen Energy 36 (2011) 12381–12392.
[9] D. Lee, J. Bae, Int. J. Hydrogen Energy 37 (2012) 422–435.
[10] Z.G. Zhan, C. Wang, W.G. Fu, M. Pan, Int. J. Hydrogen Energy 37 (2012) 1094–1105.
[11] Z.J. Lu, M.M. Daino, C. Rath, S.G. Kandlikar, Int. J. Hydrogen Energy 35 (2010) 4222–4233.
[12] Z.J. Lu, C. Rath, G.S. Zhang, S.G. Kandlikar, Int. J. Hydrogen Energy 36 (2011) 9864–9875.
[13] K. Jiao, J. Park, X.G. Li, Appl. Energy 87 (2010) 2770–2777.
[14] K. Nishida, M. Ishii, S. Tsushima, S. Hirai, J. Power Sources 199 (2012) 155–160.
[15] M. Wang, K.W. Feindel, Steven, H. Bergens, R.E. Wasylishen, J. Power Sources 195 (2010) 7316–7322.
[16] P.S. Thamboon, P. Buaphad, C. Thongbai, J. Saisud, K. Kusoljariyakul, M.W. Rhodes, T. Vilaithong, Nucl. Instrum. Methods Phys. Res. A 637 (2011) S161–S164.
[17] T. Sasabe, P. Deevanhxay, S. Tsushima, S. Hirai, J. Power Sources 196 (2011) 8197–8206.
[18] P. Kr Ügera, H. Mark Öter, J. Haußann, M. Klagesa, T. Arlt, J. Banhart, C. Hartnig, I. Mankeb, J. Scholta, J. Power Sources 196 (2011) 5250–5255.
[19] K. Takada, Y. Ishigami, J. Inukai, Y. Nagumo, H. Takano, H. Nishided, M. Watanabe, J. Power Sources 196 (2011) 2635–2639.
[20] Y.S. Chen, H. Peng, J. Power Sources 185 (2008) 1179–1192.
[21] K.H. Hou, C.H. Lin, M.D. Ger, S.W. Shiah, H.M. Chou, Int. J. Hydrogen Energy 37 (2012) 3890–3896.
[22] B. Dokkar, N.E. Settou, O. Imine, N. Saifi, B. Negrou, Z. Nemouchi, Int. J. Hydrogen Energy 36 (2011) 4220–4227.
[23] C.Z. Qin, D. Rensink, S. Fell, S. Majid Hassanizadeh, J. Power Sources 197 (2012) 136–144.
[24] T. Berning, M. Odgaard, S.K. Kær, J. Power Sources 196 (2011) 6305–6317.
[25] N.S.M. Hassan, W.R. Daud, K. Sopian, J. Sahari, J. Power Sources 193 (2009) 249–257.
[26] A.D. Le, B. Zhou, J. Power Sources 193 (2009) 665–683.
[27] J.E. Dawes, N.S. Hanspal, O.A. Family, A. Turan, Chem. Eng. Sci. 64 (2009) 2781–2794.
[28] R. Wu, X. Zhu, Q. Liao, H. Wang, Y.D. Ding, J. Li, D.D. Ye, Int. J. Hydrogen Energy 35 (2010) 7588–7593.
[29] B. Markicevic, N. Djilali, J. Power Sources 196 (2011) 2725–2734.
[30] A. Casalegno, F. Bresciani, G. Groppi, R. Marchesi, J. Power Sources 196 (2011) 10632–10639.
[31] L.X. Hao, H.M. Yu, J.B. Hou, W. Song, Z.G. Shao, B.L. Yi, J. Power Sources 177 (2008) 404–411.
[32] Y. Tabe, Y. Lee, T. Chikahisa, M. Kozakai, J. Power Sources 193 (2009) 24–31.
[33] A.A. Shah, G.S. Kim, W. Gervais, A. Young, K. Promislow, J. Li, S. Ye, J. Power Sources 160 (2006) 1251–1268.
[34] N. Zamel, X.G. Li, J. Becker, A. Wiegmann, Int. J. Hydrogen Energy 36 (2011) 5466–5478.
[35] A. Esposito, C. Pianesea, Y.G. Guezennec, J. Power Sources 195 (2010) 4149–4159.
[36] P. Quan, B. Zhou, A. Sobiesiak, Z.S. Liu, J. Power Sources 152 (2005) 131–145.
[37] Z.G. Zhan, J.S. Xiao, M. Pan, R.Z. Yuan, J. Power Sources 160 (2006) 1–9.
[38] K. Jiao, B. Zhou, P. Quan, J. Power Sources 154 (2006) 124–137.
[39] N. Akhtar, P.J.A.M. Kerkhof, Int. J. Hydrogen Energy 36 (2011) 3076–3086.
[40] H. Kim, J.H. Nam, D. Shin, T.Y. Chung, Y.G. Kim, Curr. Appl. Phys. 10 (2010) S91–S96.
[41] A.D. Le, B. Zhou, Electrochim. Acta 54 (2009) 2137–2154.
[42] P. Quan, M.C. Lai, J. Power Sources 164 (2007) 222–237.
[43] Y. Ding, H.T. Bi, D.P. Wilkinson, J. Power Sources 196 (2011) 6284–6292.
[44] X. Zhu, P.C. Sui, N. Djilali, J. Power Sources 172 (2007) 287–295.
[45] X. Zhu, P.C. Sui, N. Djilal, Microfluid Nanofluid 4 (2008) 543–555.
[46] X. Zhu, P.C. Sui, N. Djilali, J. Power Sources 181 (2008) 101–115.
[47] A.D. Le, B. Zhou, H.R. Shiu, C.I. Lee, W.C. Chang, J. Power Sources 195 (2010) 7302–7315.
[48] Y. Ding, H.T. Bi, D.P. Wilkinson, J. Power Sources 195 (2010) 7278–7288.
[49] ANSYS 12. 1 Documentation, 2009.
[50] S. Litster, D. Sinton, N. Djilali, J. Power Sources 154 (2006) 95–105.
[51] A. Bazylak, D. Sinton, Z.S. Liu, N. Djilali, J. Power Sources 163 (2007) 784–792.
[52] A. Bazylak, J. Heinrich, N. Djilali, D. Sinton, J. Power Sources 185 (2008) 1147–1153.